NUCLEAR INSTRUMENTS AND METHODS 135 (1976) 319–330; © NORTH-HOLLAND PUBLISHING CO.

EFFICIENCY AND SPATIAL RESOLUTION MEASUREMENTS OF A MODULAR NEUTRON DETECTOR IN THE KINETIC ENERGY RANGE 15–120 MeV

G. BETTI, A. DEL GUERRA, A. GIAZOTTO, M A. GIORGI, A. STEFANINI

Istituto di Fisica dell'Università, Piazza Torricelli 2, I-56100 Pisa, Italy and
Istituto Nazionale di Fisica Nucleare, Sezione di Pisa, Via Livornese, S Piero a Grado, I-56010 Pisa, Italy

D. R BOTTERILL, D W BRABEN*, D. CLARKE and P. R. NORTON

Daresbury Laboratory, Daresbury, Warrington WA4 4AD, England

Received 16 March 1976

The detection efficiency of a 3 × 3 matrix of NE 110 scintillator blocks, 153 × 153 × 270 mm long, has been measured in the neutron kinetic energy range 15–120 MeV for several thresholds, ranging from 2.80 to 15 75 MeV equivalent electron energy, and for various thicknesses of lead shielding in front of the counter. The probabilities of detecting a neutron in a block different from the one struck by the beam ('mixing') and in more than one block ('multifiring') have also been measured as a function of threshold and shielding. Comparisons have been made with a Monte Carlo program which accounts for the modular structure of the counter The efficiency and the spatial resolution of a very large matrix have been obtained, using both experimental and Monte Carlo results.

1. Introduction

In previous papers[1,2]) we described a large aperture 145 element neutron counter (PEP counter) used in a series of electroproduction experiments at the Daresbury Laboratory Synchrotron NINA. Prior to finalizing its design, a prototype counter consisting of only 9 elements was constructed and an extensive series of efficiency measurements carried out using the neutron time-of-flight (TOF) facility at UKAEA Harwell. The module was sufficiently manœuvrable to be placed at any desired position relative to the incident neutron beam and yet large enough to allow extrapolation of the results to the PEP counter.

The performance of the module was studied for several thresholds and shielding configurations in the neutron kinetic energy range (E) 15–120 MeV. The finely collimated neutron beam enabled us to investigate in detail how the efficiency and the spatial resolution depended on the modular structure of the counter.

A Monte Carlo program was written[3]) and its predictions compared with the experimental measurements. Good agreement was obtained, and the Monte Carlo was subsequently used to extrapolate the experimental results to higher energy.

The paper is organized as follows:
section 2 briefly describes the experimental apparatus and the running conditions. In section 3 the results of the efficiency measurements are presented, together with a discussion of the 'mixing' and 'multifiring' effects; the 'effective' absorption cross section of neutrons in lead is also derived. Section 4 outlines the relevant features of the Monte Carlo program and a comparison is made with the measured efficiency Finally in section 5 the efficiency and spatial resolution of the PEP counter are deduced for the running conditions of the Daresbury electroproduction experiments.

* Present address The Cabinet Office, Whitehall, London, England

2. Experimental technique

The technique used to measure the efficiency, $\eta_{\mathrm{Mod}}(E)$, was very simple; the number of neutrons detected in the module to be calibrated, $N_{\mathrm{Mod}}(E)$, was compared with the number of neutrons detected in a reference counter, $N_{\mathrm{RC}}(E)$, of known efficiency, $\eta_{\mathrm{RC}}(E)$, for the same number of incident neutrons The efficiency was then given by

$$\eta_{\mathrm{Mod}}(E) = \frac{N_{\mathrm{Mod}}(E)}{N_{\mathrm{RC}}(E)}\,\eta_{\mathrm{RC}}(E).$$

2.1. Experimental apparatus

The Harwell TOF spectrometer has been fully described elsewhere[4]). Basically the neutron beam was produced by deflecting the 143 MeV proton burst onto a thin Al target, and the neutrons and the γ-rays produced were collimated along a 50 m flight path to a size of 20 × 20 mm^2 at the position of the counter to

be tested. A scan across the beam with a thin scintillation counter gave the beam dimensions.

The TOF start pulse was derived from the beam deflection system of the synchrocyclotron and triggered a gated oscillator clocking pulses into a 300 MHz scaler; the TOF stop was provided by the neutron detector. A typical TOF spectrum is shown in fig. 1. The γ peak, evident in the first few channels, was used for calibrating the TOF origin. Details of the fast electronics are given in ref 5

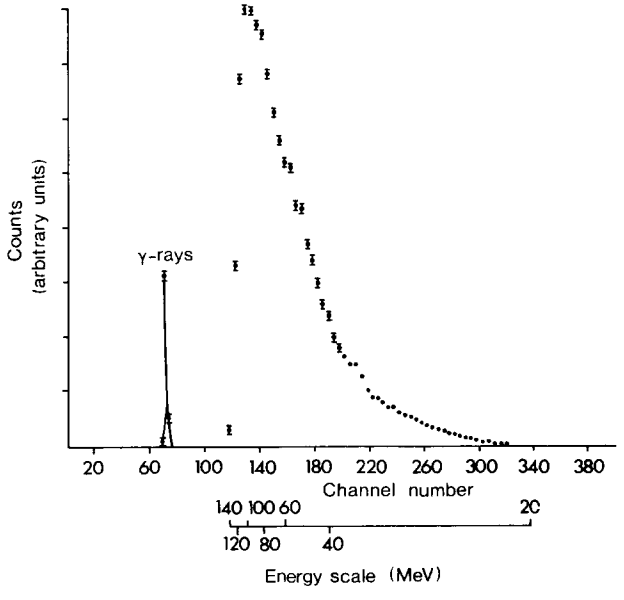

Fig 1. Typical time-of-flight spectrum.

The neutron detector (fig 2) consisted of a 3×3 array of NE 110 scintillator blocks $153 \times 153 \times 270$ mm long contained in a crate structure formed by interlocking black perspex sheets 6.35 mm thick Each scintillator was viewed by an RCA 8575 photomultiplier through an air light guide that was simply an extension of the scintillator compartment coated with diffusive reflecting paint. The module was mounted on a stand provided with vertical and horizontal movements and was able to rotate around a vertical axis.

The reference counter used a cylindrical scintillator 177.8 mm long and 76 2 mm in diameter; its threshold was kept constant throughout the experiment at 3 0 MeV equivalent proton energy where its efficiency had been measured[6]) The relative intensity of the neutron beam was monitored with a 10 mm thick scintillation counter left permanently in the beam

The data acquisition system was capable of handling only one event per burst. The data for each event, namely TOF and pattern of the blocks firing in the neutron detector, were stored on magnetic tape via a DDP 516 computer[7]). A limited on-line inspection of a sample of the data was possible The complete analysis was performed off-line.

2.2. Running conditions

The detection threshold of each counter was set at a level corresponding to the mid-point of the experimental Compton edge of the ThC″ (^{208}Tl) γ-ray spectrum; the maximum energy of this source is 2.615 MeV, giving a maximum recoil electron energy of 2.40 MeV Following a method suggested by Chikkur and Umakantha[8]), the actual threshold setting was deter-

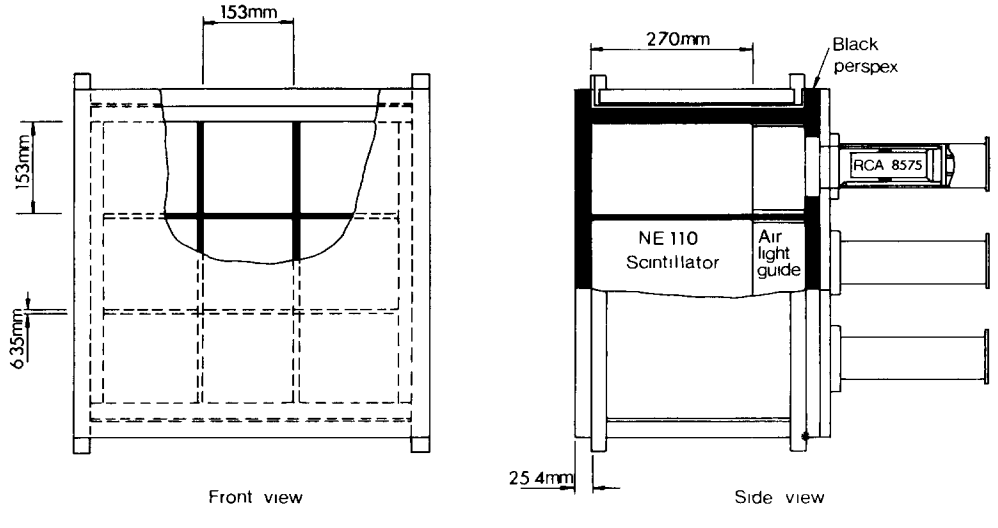

Fig. 2 Schematic of neutron counter module.

mined to be (2 8 ± 0.32) MeV. This value was checked a posteriori with the Monte Carlo program as explained in section 4. Variable attenuators were then used to reproduce higher thresholds

Most of the measurements were made with the neutron beam incident normally on the centre of the module ('standard illumination' condition). The efficiency was measured for several detection thresholds, namely, 2.80, 5.58, 7.89, 11.15, and 15.75 MeV equivalent electron energy (eq el. en.) which corresponded to attenuator settings of 0, 6, 9, 12 and 15 dB. These values corresponded approximately to 7.0, 11.5, 14.8, 19.5 and 26 7 MeV equivalent proton energy as obtained using the parametric formula of Craun and Smith[9]). This threshold scan was repeated for 1, 2 and 3 inches of lead shielding in front of the detector together with a perspex-iron-perspex sandwich, each layer 10 mm thick, to simulate the veto counter system of the PEP counter[1, 2]). In the rest of the paper we refer to these three shielding conditions as 1, 2 and 3 inches of lead and to the condition with no shielding at all as the bare counter.

The detection efficiency of the module was also studied as a function of both the impact position and the angle of incidence of the neutron beam. This set of measurements was made at a threshold of 11.15 MeV eq. el. en. and with 2″ of lead since this was the most likely running condition for the electroproduction experiments.

Frequent runs were made with the reference counter in order to monitor the neutron energy spectrum and the TOF origin.

Typically 10^4 monitor counts were taken for each run; this corresponded to ~20 min running time and on average 5×10^4 events were recorded in the module or in the reference counter. Since the chosen intensity at the counter was a few neutrons/burst, the dead-time correction[10]) applied was rather small, i.e. of the order of a few percent at the extreme end of the TOF spectrum where the correction was maximum.

The experimental results were grouped in 5 MeV energy bins over the range $10 \leqslant E \leqslant 135$ MeV. The energy resolution varied from 1.1% at 15 MeV to 3 2% at 135 MeV. For statistical reasons the maximum energy accepted was limited to 120 MeV; the statistical error on the measured efficiency was typically ±3%

TABLE 1

Total efficiency of the module for the bare counter condition ($\times 10^2$)

E (MeV) \ Threshold (MeV eq el en)	2 80	5.58	7.89	11.15	15.75
10	26.44 ± 0.72	1.17 ± 0.13	0 12 ± 0 04	0.16 ± 0.03	0.10 ± 0 02
15	35 01 ± 0.96	11.46 ± 0.49	2 03 ± 0.20	0 26 ± 0.04	0 20 ± 0.04
20	33.03 ± 0.93	17.30 ± 0 62	10.39 ± 0.47	1 84 ± 0.12	0.02 ± 0 01
25	31 37 ± 0.87	19 61 ± 0.65	12 26 ± 0.50	6 94 ± 0 24	0.60 ± 0 06
30	37.25 ± 0.99	23 13 ± 0.73	14 48 ± 0.56	11 10 ± 0 33	4.27 ± 0.19
35	38.19 ± 0.99	23 55 ± 0.74	19 03 ± 0.65	12.85 ± 0.36	8.30 ± 0.27
40	36 61 ± 0.96	25 71 ± 0 77	19 52 ± 0.65	15 36 ± 0.40	9.87 ± 0 30
45	35 72 ± 0.93	26 35 ± 0 77	20 41 ± 0.66	17 19 ± 0.42	11.58 ± 0.33
50	36.11 ± 0 94	28 07 ± 0 80	23.11 ± 0 71	17.95 ± 0.43	14 08 ± 0 37
55	33.77 ± 0 89	27 26 ± 0 77	22 22 ± 0.68	18 50 ± 0.44	14.77 ± 0 38
60	33.01 ± 0.88	27 81 ± 0 79	22.76 ± 0 70	19.89 ± 0.47	16.52 ± 0.41
65	31.76 ± 0 87	25.98 ± 0 76	24 04 ± 0.73	20.81 ± 0.48	17.21 ± 0.42
70	31 82 ± 0 88	25.39 ± 0.77	22 26 ± 0 70	21.26 ± 0.50	18 85 ± 0.46
75	30.70 ± 0.87	26.25 ± 0.79	24 00 ± 0.75	21.78 ± 0 52	19 58 ± 0 48
80	30.07 ± 0.87	26 63 ± 0.81	24.33 ± 0 76	21.84 ± 0.52	20.26 ± 0 50
85	29.76 ± 0 87	26 69 ± 0.81	23 63 ± 0.75	22 26 ± 0.54	19 35 ± 0 48
90	29.48 ± 0 88	24.93 ± 0 79	21.99 ± 0.73	22 28 ± 0.55	20 73 ± 0 52
95	29.16 ± 0.89	24 56 ± 0 79	22 29 ± 0.74	21 82 ± 0 55	20 87 ± 0 53
100	29.97 ± 0 94	25 72 ± 0 85	23.65 ± 0 81	22 48 ± 0 58	21 45 ± 0.56
105	29 01 ± 0 97	25 01 ± 0 88	22.86 ± 0.82	21.48 ± 0.59	20.85 ± 0.56
110	30.14 ± 1 05	25.08 ± 0 90	23.17 ± 0.86	22 42 ± 0.62	21.62 ± 0 60
115	30 50 ± 1.08	25.38 ± 0.96	23.87 ± 0 93	21 62 ± 0.64	22.20 ± 0 65
120	30 05 ± 1.18	25 20 ± 1 06	26 60 ± 1.07	22 04 ± 0.70	21.40 ± 0.68

3. Experimental results

3.1. Efficiency

The detection efficiencies measured under 'standard illumination' condition for the different threshold and shielding conditions are listed in tables 1–4 The efficiency for the bare counter at three threshold values, 2.80, 5.58 and 11.15 MeV eq el en., is shown in fig 3, together with the Monte Carlo computations, which will be discussed in section 4. At the lowest threshold, the well-known behaviour of neutron counter efficiency is shown, with a dip at ~25 MeV due to the rapidly decreasing n–p elastic cross section and to the onset of the neutron-carbon inelastic interaction*. At higher threshold values the shape of the efficiency curve follows that of the n–C inelastic cross section. The dependence on the threshold becomes less important as the kinetic energy of the neutron increases and the efficiencies tend to the same value which compare rather well with the empirical one of 1%/cm.

The decrease in efficiency with increasing lead shielding is illustrated in fig. 4 for a detection threshold of 11.15 MeV eq. el. en. The neutron–lead interaction has two components: (1) the elastic n–Pb scattering, which causes mainly a distortion of the neutron energy spectrum by decreasing the neutron energy, (2) the inelastic n–Pb scattering. The latter can be divided into two processes: a diffractive-like excitation of the nucleus, with low momentum transfer to the lead, and absorption of the neutron. Since, as fig. 3 shows, apart from the very low threshold condition, the efficiency is rather independent of the energy in the range 30–120 MeV, one may expect that both the elastic and diffractive-like n–Pb interactions do not affect the measured efficiency. Using this assumption, one can deduce an 'effective' absorption cross section of neutrons in lead, σ'_{Pb}, by simply comparing the efficiencies for different lead shielding thicknesses. With a straightforward notation one has

$$N_{\Delta X}(E) = N_0(E) \exp\left\{-\frac{\mathcal{N}\delta}{A}\,\Delta X\,\sigma'_{Pb}(E)\right\},$$

where $N_0(E)$ is the incident neutron spectrum, $N_{\Delta X}(E)$

* For a full discussion of neutron interactions in scintillator see ref 11

Table 2

Total efficiency of the module for 1″ of lead condition ($\times 10^2$).

E (MeV) \ Threshold (MeV eq el. en)	5 58	7.89	11 15	15.75
10	0 82±0 07	0.20±0 03	0.17±0 03	0.09±0 02
15	7.59±0.26	1.50±0.11	0 44±0 06	0.12±0.03
20	12.40±0.36	6.73±0.25	1.25±0.10	0.02±0.01
25	13.84±0 37	9 84±0.30	4 92±0 20	0.23±0 04
30	16.79±0.43	11.72±0 34	8 24±0.27	2 76±0.15
35	19.62±0.47	14.49±0.39	10 10±0.31	5 22±0.21
40	20.82±0.49	17 22±0.43	12.05±0.34	6.33±0.23
45	21 06±0 49	17.91±0.43	13 84±0.37	8 18±0 26
50	23 03±0.52	18.78±0.45	14.70±0 39	9.71±0 29
55	22.44±0.50	18.75±0.44	15 09±0 38	11 00±0.31
60	23 13±0.52	20 41±0 47	16.08±0.40	12 31±0.34
65	23.71±0.53	21.68±0.50	16 89±0.42	12 58±0.35
70	24.09±0.54	20.45±0.48	17 30±0 43	14.07±0.37
75	24 49±0.56	22.49±0 53	18.47±0 46	15.28±0.40
80	24.37±0.57	21.76±0 52	19.82±0 49	16.09±0.42
85	24.68±0.58	22.30±0.53	19 50±0.49	15.63±0 42
90	25.17±0.60	22.47±0.55	19.36±0.49	16.44±0.44
95	23 89±0.58	21.79±0 55	18.52±0 48	16.81±0 45
100	24 34±0 61	23 00±0 59	19 94±0 53	18 23±0.50
105	24.37±0.62	22.85±0.59	20 30±0 55	17 35±0.49
110	24.86±0 66	23.44±0.64	20 03±0 57	18 76±0.54
115	24.17±0 69	23 83±0.68	20 25±0 61	18 40±0.57
120	25 70±0.78	24 57±0.68	20 33±0 66	19 51±0.64

TABLE 3

Total efficiency of the module for 2″ of lead condition ($\times 10^2$).

E (MeV) \ Threshold (MeV. eq el. en)	5.58	7.89	11.15	15 75
10	0.81 ± 0.07	0 18 ± 0.03	0.25 ± 0.05	0 10 ± 0.02
15	6 14 ± 0.23	1.34 ± 0.13	0 41 ± 0 09	0 16 ± 0.04
20	10.40 ± 0 32	6.03 ± 0.23	1.13 ± 0 09	0.03 ± 0 01
25	11 61 ± 0.33	8 08 ± 0.27	4.63 ± 0 19	0.31 ± 0 05
30	14 16 ± 0 38	10 50 ± 0 32	6 91 ± 0 25	2 40 ± 0 14
35	16.36 ± 0.42	12.89 ± 0.36	8.29 ± 0.27	4.45 ± 0 19
40	18.47 ± 0.45	14 00 ± 0.37	9.82 ± 0.30	5 58 ± 0 21
45	18.71 ± 0 45	15 43 ± 0 39	11 64 ± 0 32	7.31 ± 0.25
50	19.88 ± 0.47	16.17 ± 0.41	12.58 ± 0.34	8 82 ± 0.27
55	19 47 ± 0.45	16 83 ± 0 41	13.11 ± 0.37	9 42 ± 0 28
60	21.10 ± 0.49	18.11 ± 0.44	14.57 ± 0.38	10.70 ± 0.31
65	20 91 ± 0 49	18 41 ± 0.45	14 95 ± 0.38	11.71 ± 0 33
70	21 01 ± 0 49	19.27 ± 0 46	15.24 ± 0 40	12.36 ± 0.34
75	21.89 ± 0 56	20.43 ± 0.54	16.10 ± 0.42	13.61 ± 0 42
80	22.76 ± 0.54	21.59 ± 0.52	17 76 ± 0 45	14.85 ± 0.40
85	22 20 ± 0.53	20.29 ± 0.50	17.27 ± 0.44	14.67 ± 0.40
90	22.47 ± 0 55	19.96 ± 0.51	17.42 ± 0.45	15 19 ± 0 42
95	21.71 ± 0 54	20.77 ± 0.53	17 64 ± 0 47	15 33 ± 0 43
100	23 53 ± 0 60	21.02 ± 0.55	18 28 ± 0.50	16 23 ± 0 46
105	22.63 ± 0 59	21.47 ± 0 57	17.46 ± 0.49	15.73 ± 0 46
110	23.23 ± 0.63	21.10 ± 0.59	18.12 ± 0.53	16.62 ± 0 50
115	24.26 ± 0.69	22.29 ± 0.65	18.06 ± 0 56	16 62 ± 0.53
120	25 42 ± 0.77	22.00 ± 0.70	17.41 ± 0.59	17.90 ± 0 60

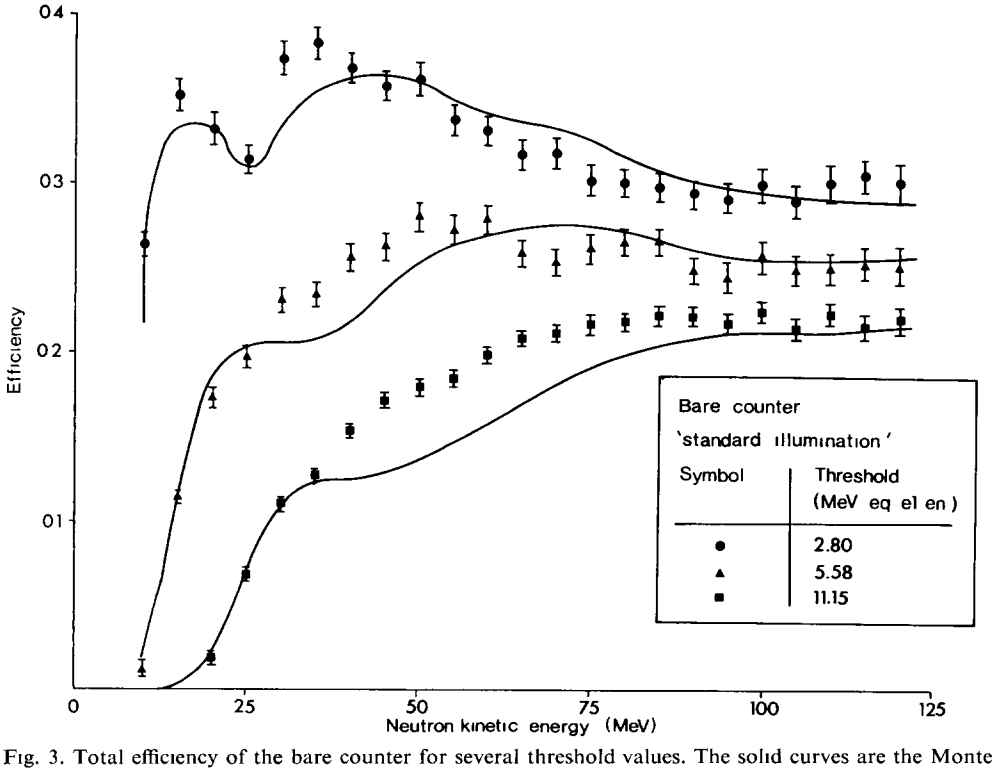

Fig. 3. Total efficiency of the bare counter for several threshold values. The solid curves are the Monte Carlo predictions.

TABLE 4

Total efficiency of the module for 3″ of lead condition ($\times 10^2$).

E (MeV) \ Threshold (MeV eq el. en)	7.89	11.15	15.75
10	0.22 ± 0 03	0 11 ± 0.02	0 08 ± 0.02
15	1 03 ± 0.09	0 25 ± 0 05	0.10 ± 0.03
20	4 64 ± 0.20	1 04 ± 0.09	0 08 ± 0 03
25	6 61 ± 0.24	3.74 ± 0.17	0.30 ± 0.05
30	8 21 ± 0.27	5 95 ± 0.23	2.00 ± 0.13
35	10 58 ± 0.32	7.12 ± 0.25	3.87 ± 0.18
40	11.77 ± 0.33	8.60 ± 0.28	4.81 ± 0.20
45	12.30 ± 0.34	10.25 ± 0.30	6 02 ± 0.22
50	13 98 ± 0.37	11 37 ± 0 32	7 37 ± 0 25
55	14.40 ± 0 37	12 08 ± 0 33	8 08 ± 0.26
60	15.56 ± 0 39	13.13 ± 0 35	9.62 ± 0.29
65	15.71 ± 0.40	13 21 ± 0.36	10 11 ± 0.30
70	16 66 ± 0 42	14 32 ± 0.38	10 55 ± 0 31
75	17 06 ± 0 47	15.03 ± 0 45	11.71 ± 0 38
80	17.46 ± 0.45	15.23 ± 0.41	12.87 ± 0.37
85	17 74 ± 0.45	15 63 ± 0.42	13.43 ± 0.38
90	17.98 ± 0.45	16.29 ± 0.44	13.79 ± 0.39
95	18.16 ± 0.48	16 18 ± 0.44	13.81 ± 0 40
100	19.36 ± 0.52	17.37 ± 0.48	14.82 ± 0 43
105	17.92 ± 0.50	17.18 ± 0.49	14.37 ± 0.43
110	18.82 ± 0.54	16.90 ± 0 48	15.23 ± 0.47
115	19.26 ± 0.59	17.39 ± 0.55	15 02 ± 0.49
120	18.36 ± 0.61	17.44 ± 0.59	15 25 ± 0 54

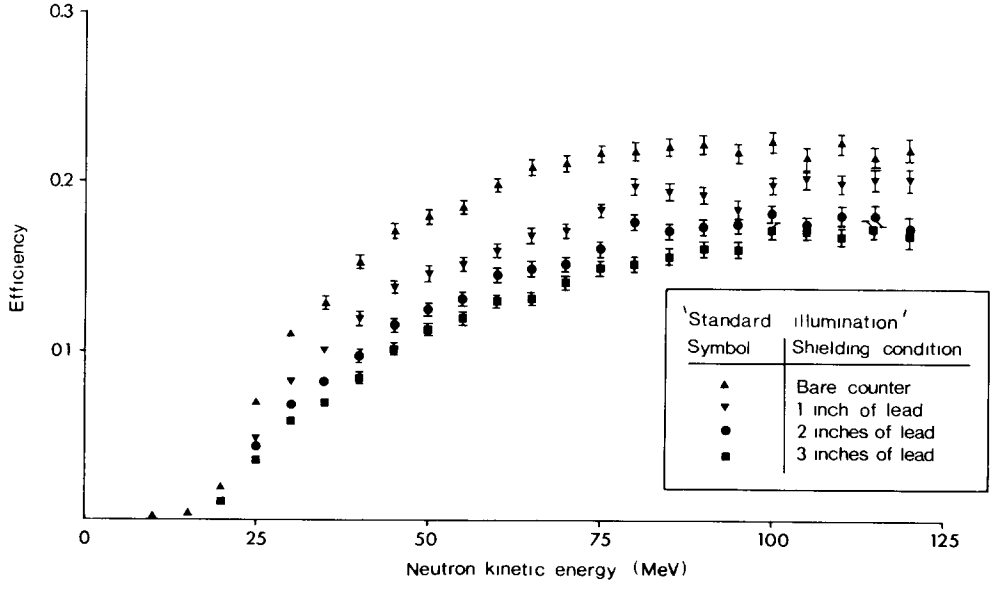

Fig. 4. Total efficiency of the module, for several shielding conditions at a threshold of 11 15 MeV eq. el. en.

is the spectrum after traversing a thickness ΔX of lead, A and δ are the atomic number and density of lead respectively and $\mathcal{N}$ is Avogadro's number.

By comparing the experimental efficiencies for 3″ and 2″ of lead and for 2″ and 1″ and taking the weighted average between the two values, $\sigma'_{Pb}(E)$ was obtained in the energy range 30–120 MeV. As expected, $\sigma'_{Pb}(E)$ was found to be independent, within the experimental errors, of the threshold value and was therefore averaged over the different threshold conditions. In fig. 5, $\sigma'_{Pb}(E)$ is reported together with the experimental values for σ_{Pb}^{inel} taken from refs 12–14. The ratio $R = \sigma'_{Pb}(E)/\sigma_{Pb}^{inel}(E)$ is nearly independent of energy and its weighted value is equal to 0.67 ± 0.01.

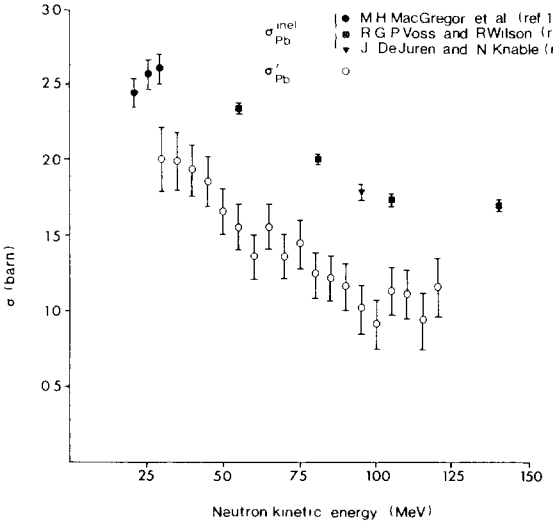

Fig. 5. 'Effective' absorption cross section for neutrons in lead compared with the experimental values of the total inelastic n–Pb cross section, taken from refs. 12–14.

The dependence of the efficiency on the impact position and the angle of incidence of the neutron was studied for 2″ of lead and for a threshold of 11.15 MeV eq. el. en. The response of the module was investigated both as 'single block efficiency', i.e. the absolute efficiency of the block struck by the beam and as the total efficiency of the whole module.

Fig. 6a shows the 'single block efficiency' for three different blocks with the beam entering normally at the centre of each block. The broad agreement exhibited shows the reproducibility of the threshold setting procedure, whilst the slightly higher efficiency of the central block could be due to the larger in-scattering contribution from the surrounding blocks The total efficiency of the module, fig. 6b, shows a much greater variation for the same impact positions.

The 'single block efficiency' for the beam entering the central block at different positions is shown in

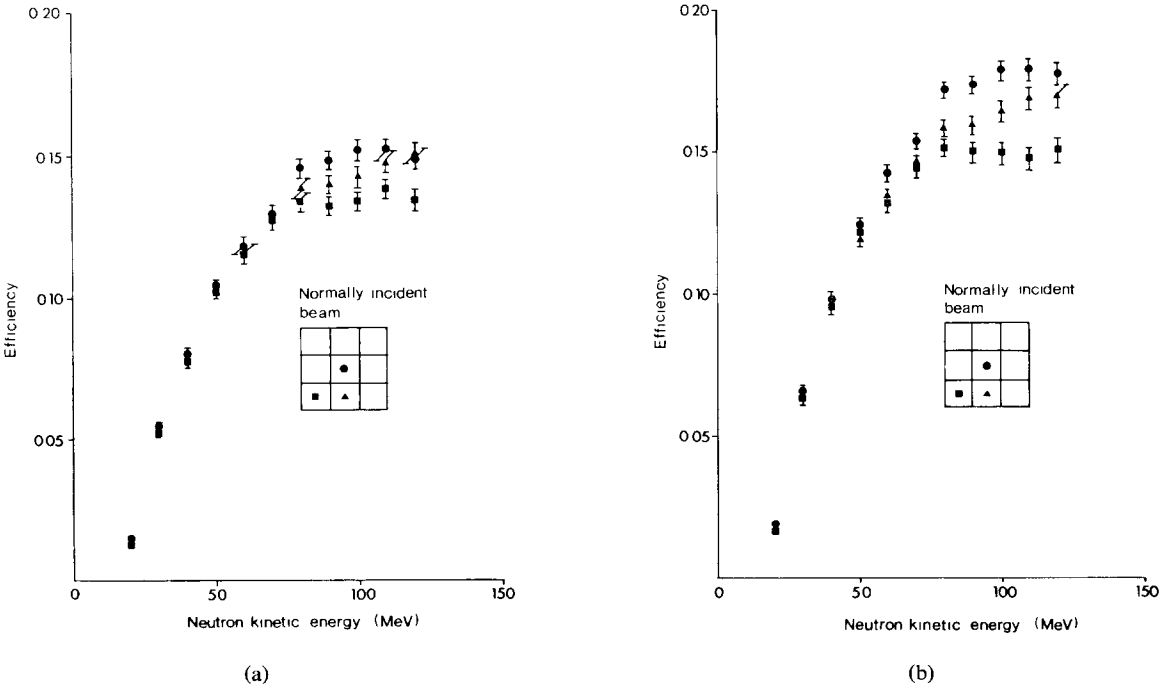

Fig 6 Efficiency for different impact positions for 2″ of lead at a threshold of 11.15 MeV eq el. en: (a) 'single block' efficiency, (b) total efficiency of the module

fig. 7, the marked difference between the various curves being now due to edge effects. On the other hand, we could find no appreciable dependence of the total efficiency on the position of the beam inside the central block.

In order to reproduce the illumination conditions of the electroproduction experiments, several runs were made with the beam entering at the centre of the module, with the angle of incidence varying from 0° to 14°. Whereas there was a slight change in the 'single block efficiency' of the central block, due to obvious geometrical effects, we found no appreciable angular dependence of the total efficiency of the module. The angular spread introduced by the elastic n-Pb scattering probably masked the $1/\cos\theta$ dependence which one would expect assuming the efficiency to be proportional to the linear dimension of the scintillator.

The effect of shielding (100 mm of lead) close behind the counter was also studied; no significant back-scattering contribution to the efficiency was found.

3.2. 'MIXING' AND 'MULTIFIRING'

The probabilities of detecting a neutron in a block different from the one struck by the beam ('mixing') and in more than one block ('multifiring') were measured for several thresholds and shielding thicknesses. The results presented in this section are for 'standard illumination' condition. It must be stressed that although they quantitatively depend on the geometry of our neutron detector, the qualitative considerations apply in general.

The 'mixing' probability for the bare counter is shown in fig 8 A strong dependence upon the threshold is evident at low energy, whereas at higher energy the 'mixing' probability reproduces the efficiency behaviour with threshold. The mixing effect is easy to explain: a neutron that impinges on a certain block can undergo several consecutive interactions without producing sufficient light to be detected, it may then enter a nearby block. where it is eventually detected. The mean number of consecutive interactions a neutron undergoes before being detected decreases rapidly with energy due to the decreasing n–C cross section

The 'mixing' probability in the shielded cases is much higher compared with the bare counter, as illustrated in fig 9. The n–Pb elastic interaction, which is of the order of 2 5 b over the accepted energy range, increases the mixing probability by a large amount which does not depend on threshold, as one expects, but only on the shielding thickness The noticeable

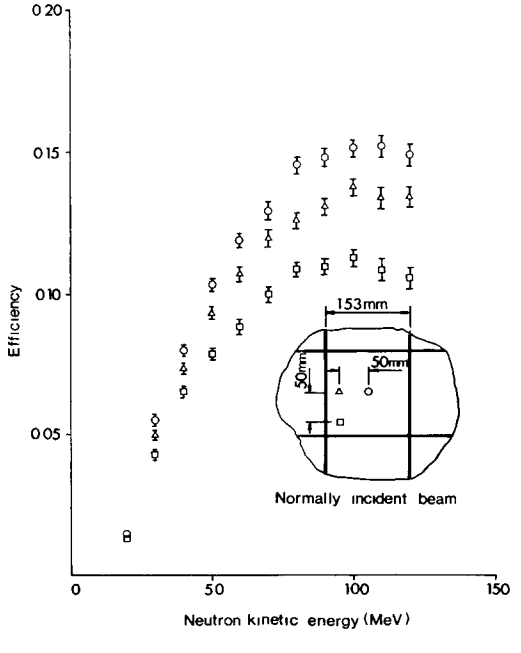

Fig. 7. Efficiency of the central block, with the beam entering at different positions, for 2″ of lead at a threshold of 11.15 MeV eq el en.

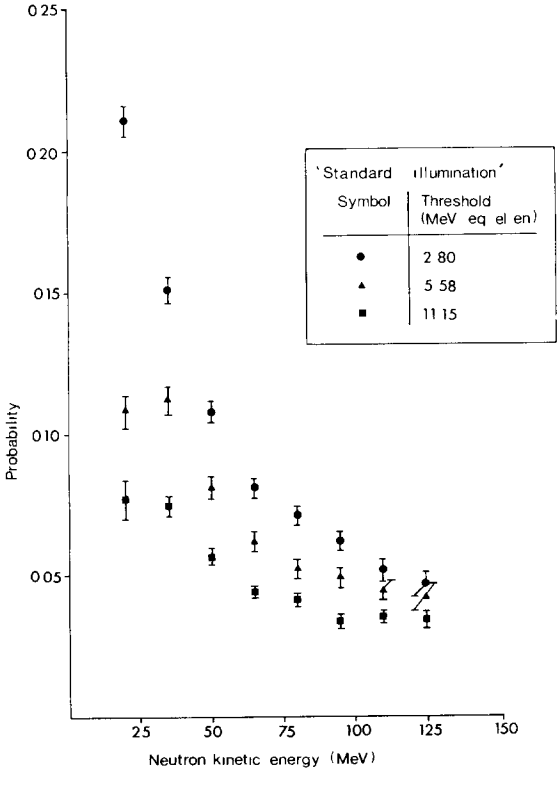

Fig 8. 'Mixing' probability for the bare counter, for several threshold values

difference between the mixing probability for the bare counter and for 1″ of lead is also due to the presence of the veto system.

'Multifiring' is mainly due to the following processes: (1) multiple interactions producing light output above the detection threshold in several blocks, (2) a single interaction producing a charged particle with sufficient energy to be detected in adjacent blocks. Results for the bare counter are shown in fig. 10; no substantial difference was found with respect to any of the shielding conditions.

Fig. 11 shows the 'mixing' and 'multifiring' probabilities averaged over the accepted energy range, for all the experimental conditions studied.

4. Monte Carlo program

The Monte Carlo program was basically a reworking in Monte Carlo form of the successful Kurtz analytical program[15]), based on the updated values of the total and differential neutron–carbon cross sections and on the most reasonable splitting among the various channels of the inelastic n–C cross section[11]). Particular care was taken to make the program as flexible as possible in order to allow a comparison to be made with the data of the various neutron detectors described in the literature. The program is applicable to cylindrical, conical, rectangular or modular geometry under any illumination conditions. The good agreement, see also ref. 11, gave us sufficient confidence to use the Monte Carlo program for extrapolating the measured efficiency to higher energy and for different illumination conditions.

4.1. Main features

The progress of a neutron inside the counter is followed to higher than second order rescattering, up to a maximum of ten interactions; any charged particle produced is also followed along its trajectory through the counter and the energy loss is calculated for a discrete number of steps of predefined length. In this way it is possible to study edge effects and for our counter specifically the effect of its modularity and of the containing perspex structure.

The light output is derived considering the different response of the scintillator to different ionizing particles.

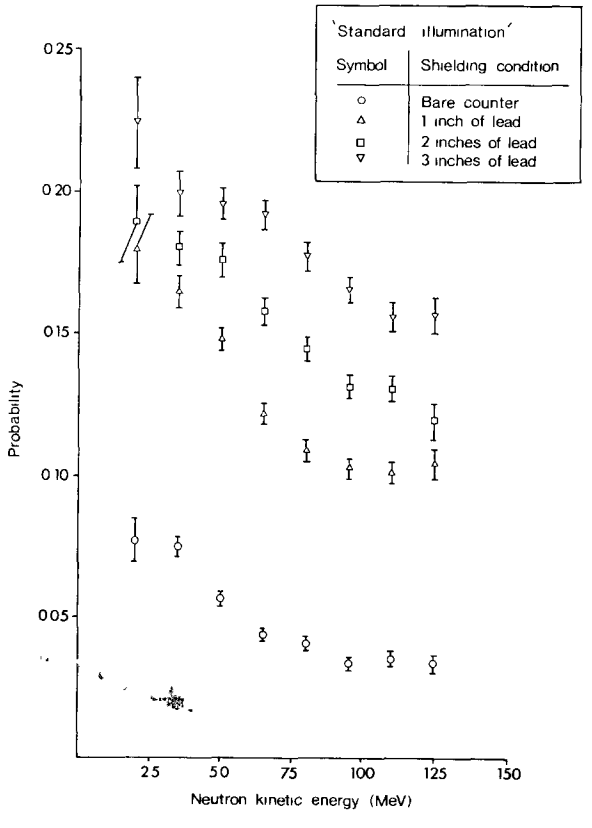

Fig. 9 'Mixing' probability for several shielding conditions at a threshold of 11.15 MeV eq. el. en.

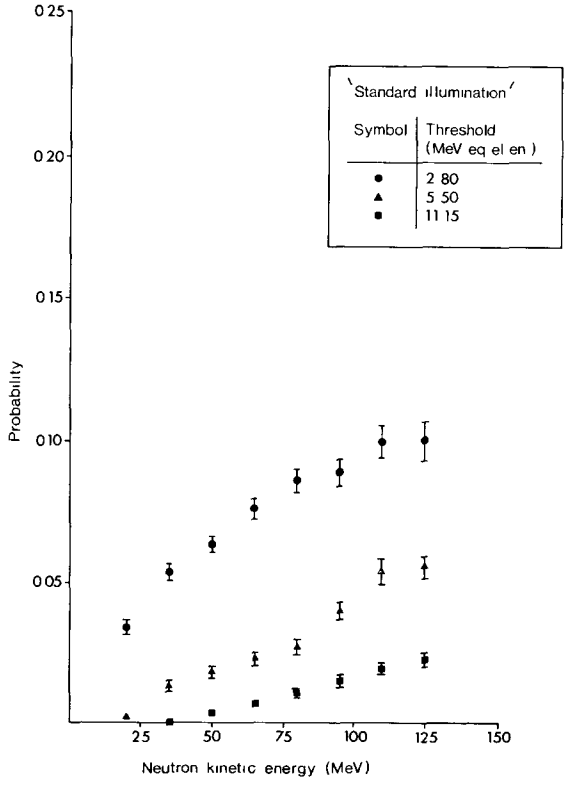

Fig. 10 'Multifiring' probability for the bare counter, for several threshold values

The program also simulates: (1) the amplitude and the time response of the overall light pulse reaching the photomultiplier, taking into account the attenuation and the transit time through the scintillator, (2) pulse shaping, e.g. clipping of photomultiplier pulses, and (3) the finite resolution of the system. The total efficiency of the counter is computed together with the contribution to the efficiency from individual cross section channels. For modular counters 'single block' efficiencies, 'mixing' and 'multifiring' probabilities are also given.

4.2. Comparison with experimental results

Monte Carlo predictions for the bare counter are presented in fig. 3, together with the measured efficiencies. Excellent agreement is obtained over the whole energy range for the lowest threshold value. The agreement is not as good between 40 and 80 MeV for the higher threshold where the somewhat arbitrary regrouping of the many n–C inelastic channels plays a critical role[11]). Nevertheless, at higher energy, the Monte Carlo gives a perfectly adequate representation of the efficiency for all threshold values

The threshold values were also checked with the Monte Carlo program The internal consistency obtained in the threshold region (fig 3) between all the experimental results and Monte Carlo predictions gave us confidence in the quoted values.

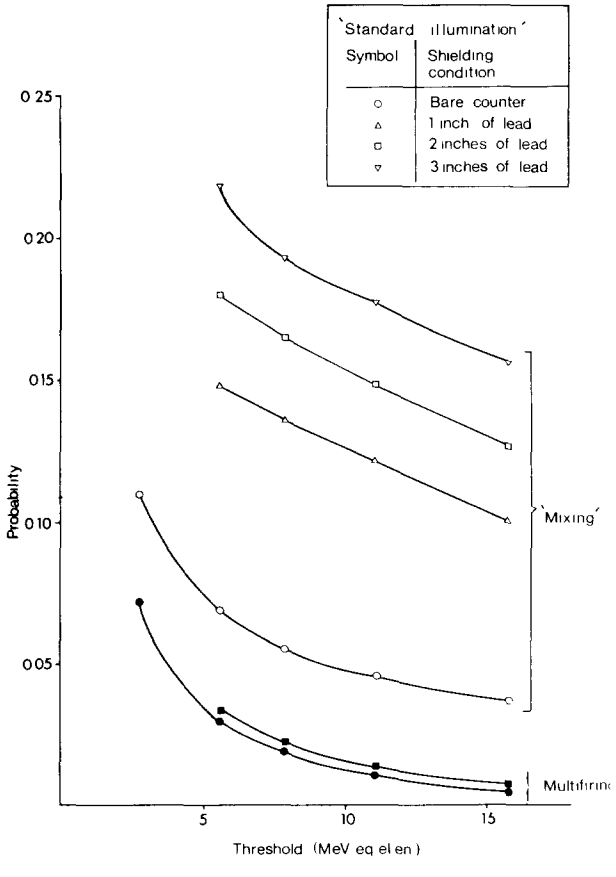

Fig. 11. 'Mixing' and 'multifiring' probabilities averaged over the energy range 15–120 MeV, as functions of threshold for various shielding conditions The solid curves are hand-fitted

4.3. Edge and perspex effects

The variation of efficiency across the counter was also investigated using the Monte Carlo program A scan was simulated with a pointlike beam incident normally to the face of the counter. Relative efficiencies for several neutron energies and two threshold values are shown in fig. 12 The main features of the results are:

1) The fall in efficiency at the edge of the scintillator is more pronounced at the higher threshold In all cases, however, 'full' efficiency is recovered in less than 1 cm from the edge, and the dependence on neutron energy is small A similar behaviour is also visible in the data of Crabb et al [16])

2) A substantial fraction ($>50\%$) of the neutrons entering the perspex is detected in one of the adjacent blocks. The influence of the perspex is slightly greater at the higher threshold value, as can be expected, and increases with decreasing energy

4 4 Extrapolation of the efficiency to higher energy

The efficiency of the shielded counter at higher energy, which needed to be known for the π^+ electroproduction experiment[17]) was derived by scaling the Monte Carlo results for the bare counter with a flux reduction factor due to the shielding This factor was calculated from the data presented in section 3.1, using the assumption that the neutron flux reduction was constant from 120 to 250 MeV, since the inelastic n–Pb cross section is also constant in that energy range A subsequent experiment[18]) made at Daresbury Laboratory, using the $\gamma p \rightarrow \pi^+ n$ process to directly measure the PEP counter efficiency at higher energy, confirmed the validity of our extrapolation

5. Efficiency and spatial resolution of a large array

The experimental and Monte Carlo results were used to deduce the efficiency and the spatial resolution of the PEP 145 element counter as described below

Assuming point-like illumination at its centre, the

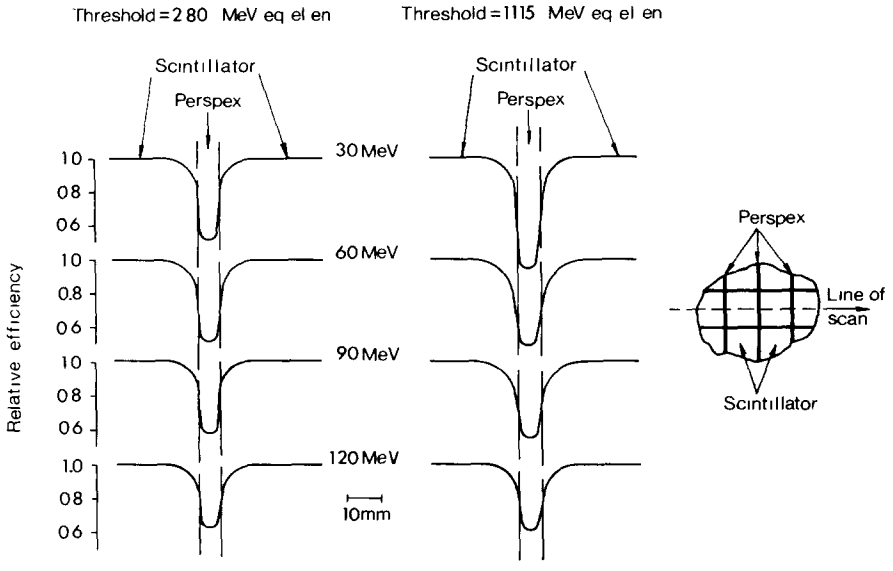

Fig. 12. Monte Carlo prediction of the relative efficiency across the counter for four neutron kinetic energies and for two threshold values

total efficiency of a matrix, η_T, for a given threshold and shielding thickness may be expressed as

$$\eta_T(E) = \sum_{i=0}^{n} \eta_i(E)$$

where η_0 is the efficiency contribution from the central block, η_1 is the contribution from the first ring surrounding the central block, and so on. Since most of the measurements were taken at a threshold of 11.15 MeV eq. el. en. and for 2″ of lead, we deduced the efficiency and the spatial resolution for this condition, using reasonable assumptions it is also possible to derive them for the other shielding thicknesses and threshold values.

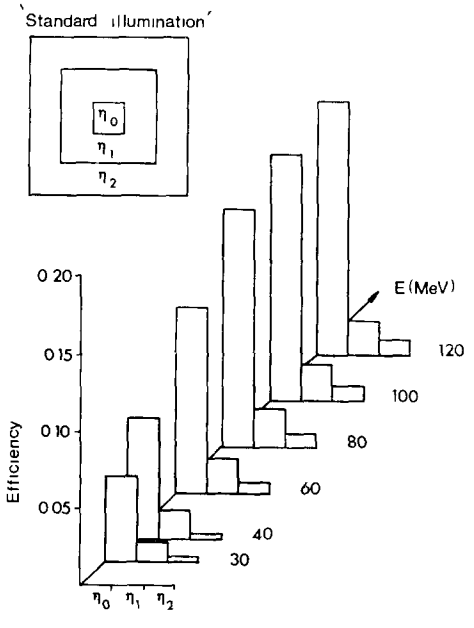

Fig. 13. Contribution to the total efficiency from η_0, η_1 and η_2, see also text, for 2″ of lead at a threshold of 11 15 MeV eq el en.

η_0 and η_1 were obtained from measurements taken with the beam entering the centre of the module; η_2 was derived from the set of measurements with the beam incident in the outer blocks, and applying obvious symmetry consideration. Fig. 13 shows η_0, η_1 and η_2 in histogram form for several energies. η_3 was then obtained by making a smooth exponential extrapolation through the last two bins of the histograms; this contribution was found to be rather small and it was assumed that the contribution from further rings was negligible. Table 5 presents the values of η_0–η_3 obtained after regrouping into larger energy bins. The errors quoted for η_1 and η_2 are not purely statistical but also include systematic effects due to in-scattering and beam geometry. The error on η_3 has been taken as large as the value of η_3 to account for the uncertainty of the extrapolation. Since the total efficiency of the module was relatively independent of the beam position within the central block, these considerations are also valid for uniform illumination conditions, providing the neutron envelope is well inside the array.

A further correction was also applied for the effect

TABLE 5

η_i as function of energy ($\times 10^2$)

E (MeV)	η_0	η_1	η_2	η_3
30	5.67±0 09	1 24±0 09	0.35±0 05	0 06±0 06
40	7 92±0.11	1 89±0.11	0.42±0 06	0.10±0.10
60	12 30±0.12	2.27±0 12	0.68±0 07	0 20±0 20
80	15.31±0 12	2 45±0.12	0.91±0 09	0 34±0.34
100	15.89±0 13	2.39±0.13	1.01±0.09	0.42±0 42
120	15 16±0 16	2.25±0 16	1.03±0 12	0 47±0.47

of the perspex structure. We have treated the perspex as a reduced efficiency scintillator with a reduction factor $\beta(E)$, as computed using the Monte Carlo program (fig. 12). Since in the matrix a volume V_p is occupied by perspex and V_S by scintillator, the efficiency for uniform illumination may be written as

$$\eta(E) = \eta_T(E)\,[1 - f_p(E)],$$

where

$$f_p(E) = \frac{V_p}{V_p + V_s}\,[1 - \beta(E)].$$

One can also write $\eta(E)$ as simply proportional to the efficiency of the module for 'standard illumination', $\eta_{Mod}(E)$, as

$$\eta(E) = \eta_{Mod}(E)\,[1 + f(E)],$$

where f is an overall correction factor Since the statistical error for η_{Mod} was of the order of 3%, $f(E)$ was averaged over the energy range 15–120 MeV, and was found to be equal to (0.0±2.5)%.

The spatial resolution was deduced from the η_i values, assuming the spatial distribution of the detected neutrons to be gaussian. The standard deviation σ as function of energy can be expressed as

$$\sigma(E) = \left[\frac{\sum_{i=0}^{n} \eta_i(E)\,\overline{r_i^2}}{\sum_{i=0}^{n} \eta_i(E)}\right]^{\frac{1}{2}},$$

where $\overline{r_i^2}$ is the mean square distance from the centre of the matrix in first block, in the first ring and so on; σ was found to be of the order of 0.9 of a block width and practically independent of the neutron kinetic energy.

We are indebted to the Harwell time-of-flight group and the synchrocyclotron team for much help while setting-up and running, in particular to A Langsford, P. H. Bowen and G. C Cox. We would also like to thank I. Edwards for his enthusiastic assistance during data taking.

References

1) G. Betti, D. R. Botterill, D. W Braben, D. Clarke, A Del Guerra, A. Giazotto, M. A Giorgi, P. R Norton and A Stefanini, Proc. Int. Conf. on *Instrumentation for high energy physics*, Frascati, May 1973 (ed S. Stipcich; CNEN, Frascati, 1973), p. 422

2) A Del Guerra, A. Giazotto, M A. Giorgi, A Stefanini, D R Botterill, D. W Braben, D Clarke and P R. Norton, Nucl Instr. and Meth. **135** (1976) 307.

3) G Betti, Thesis (University of Pisa, 1972) unpublished

4) T. P. Scanlon, G H. Stafford, J. J Thresher and P H. Bowen, Rev. Sci. Instr. **28** (1957) 749

5) A Del Guerra, M. A Giorgi, A Giazotto, A Stefanini, D. W. Braben and D. Clarke, Darebury Laboratory Internal Report DNPL/TM 75, November (1970) unpublished

6) A Langsford, private communication

7) C Whitehead, O. O. Jarvis and A Langsford, Camac Bull **4** (1972) 18

8) G C. Chikkur and N Umakantha, Nucl Instr and Meth **107** (1973) 201

9) R L. Craun and D L. Smith, Nucl. Instr and Meth. **80** (1970) 239

10) P. H Bowen, G. C Cox, G B Huxtable, A Langsford, J P. Scanlon, G. H Stafford and J J. Thresher, Nucl. Instr and Meth. **17** (1962) 117

11) A. Del Guerra, Nucl. Instr. and Meth **135** (1976) 337.

12) M. H. MacGregor, W P. Ball and R. Booth, Phys. Rev **111** (1958) 1155

13) R G P. Voss and R. Wilson, Proc. Roy. Soc. **A236** (1956) 41

14) J. DeJuren and N. Knable, Phys Rev. **77** (1950) 606

15) R. J Kurz, University of California Radiation Laboratory Report, UCRL-11339, March (1964).

16) D G Crabb, J G. McEwen, E. G. Auld and A Langsford, Nucl Instr. and Meth **48** (1967) 87

17) A Del Guerra, A Giazotto, M. A. Giorgi, A. Stefanini, D R. Botterill, D W. Braben, D. Clarke and P Norton, Nucl Phys **B99** (1975) 253

18) J Bailey, D R. Botterill, D. Clarke, H. E Montgomery, P R Norton, G. Matone, A Del Guerra, A Giazotto, M A Giorgi and A Stefanini, Nucl Instr and Meth. **135** (1976) 331